Journal of Membrane Science 675 (2023) 121532

Contents lists available at ScienceDirect

Journal of Membrane Science

journal homepage: www.elsevier.com/locate/memsci

Outstanding performance of PIM-1 membranes towards the separation of fluorinated refrigerant gases

Sergio V. Gutiérrez-Hernández [a], Fernando Pardo [a], Andrew B. Foster [b], Patricia Gorgojo [c], Peter M. Budd [b], Gabriel Zarca [a,**], Ane Urtiaga [a,*]

[a] Department of Chemical and Biomolecular Engineering, Universidad de Cantabria, Av. Los Castros 46, 39005, Santander, Spain
[b] Department of Chemistry, University of Manchester, Oxford Road, Manchester, M13 9PL, UK
[c] Departamento de Ingeniería Química y Tecnologías Del Medio Ambiente, Universidad de Zaragoza, C/ Pedro Cerbuna 12, 50009, Zaragoza, Spain

ARTICLE INFO

Keywords:
R-32
R-134a
R-1234yf
R-125
Gas separation
Polymers of intrinsic microporosity
Physical aging
Long-term performance

ABSTRACT

The recycling of depleted high global warming mixtures of fluorinated gases (F-gases) with close-boiling or azeotropic behavior requires advanced separation processes to obtain effectively the pure components. Herein, several types of PIM-1 membranes were tested for the first time towards the separation of hydrofluorocarbons and hydrofluoroolefins, showing extraordinarily high permeability coefficients for the value-added difluoromethane (R-32), up to 4100 barrer, coupled with high selectivity for the F-gas pairs of interest. Additionally, the solubility of selected F-gases in PIM-1 was measured and fitted to the dual-mode and Guggenheim, Anderson and de Boer sorption models. The separation performance of the standard PIM-1 and a highly branched PIM-1 was examined with the mixture R-410A (containing R-32 and pentafluoroethane R-125) to assess the influence of the membrane topology on the mixed-gas permeation properties over time (physical aging). Considering that the branched PIM-1 membrane was the least impacted by the aging phenomena, it was used to recover high purity R-32 (concentration in the permeate side as high as 98.9 vol % was achieved) from refrigerant gas mixtures R-410A and R–454B (mixture of R-32 and R-1234yf) in continuous long-term experiments. Results showed the great potential of PIM-1 membranes for the separation of R-32 from refrigerant mixtures collected from end-of-life equipment.

1. Introduction

The continuous growth of refrigerant greenhouse gas (GHG) emissions has led to new policies restricting the production and consumption of these substances in major industrial sectors, with the aim of mitigating their impact on climate change [1,2]. These policies impact the refrigeration and air conditioning (RAC) sector because it uses hydrofluorocarbons (HFCs), a class of fluorinated gases (F-gases) with global warming potential (GWP) ranging from several hundreds to thousands of times that of the reference CO_2. With the aim of reducing fugitive HFC emissions into the atmosphere, and aligning the RAC sector to more sustainable models, a circular economy model is proposed whereby spent blends of F-gases will be recovered and recycled in new equipment [3]. Recycling involves collecting the working fluids from end-of-life equipment and separating the refrigerant blend into its pure constituents, to take advantage of those compounds with lower GWP in the formulation of new environmentally friendly mixtures, such as those formed by HFCs and hydrofluoroolefins (HFO), a new class of refrigerants with negligible GWP.

Some of the most common HFC and HFO refrigerants, and their mixtures, used in this work are presented in Table S1 together with their chemical name and relevant physical properties. As can be seen, the separation of F-gas mixtures requires advanced separation processes to obtain effectively the pure components for recycling purposes due to their similar properties, which may lead to close-boiling mixtures (e.g., R-32 and R-1234yf) or even azeotropic systems (e.g., R-32 and R-125) [4]. In this regard, in-depth research on absorption separation processes with ionic liquids (ILs) and deep eutectic solvents has been conducted [4], as well as on the adsorption separation of F-gas mixtures with porous materials [5] such as metal organic frameworks (MOFs) [6,7], zeolites [8] and activated carbons [9]. In addition, membrane technology has been recently evaluated using rubbery polymers such as poly

* Corresponding author.
** Corresponding author.
E-mail addresses: zarcag@unican.es (G. Zarca), urtiaga@unican.es (A. Urtiaga).

https://doi.org/10.1016/j.memsci.2023.121532
Received 14 December 2022; Received in revised form 15 February 2023; Accepted 26 February 2023
Available online 27 February 2023

(ether-*b*-amide) (PEBA) [10], poly (dimethylsiloxane) and other glassy fluoropolymers such as CyclAFlor™ [11]. Among the different PEBA copolymers, Pebax 1657 provided the highest ideal gas selectivity, albeit with the lowest permeability coefficients [12], and it was further used to assess the separation of commercial refrigerant mixtures (e.g., R-410A, an equimassic mixture of R-32 and R-125). Additionally, with the aim of overcoming the trade-off between permeability and selectivity, Pebax 1657 was functionalized with ILs, leading to the so-called composite polymer-ionic liquid membranes (CPILMs), which proved to have significantly enhanced separation properties [13]. Particularly, for the separation of novel HFC/HFO mixtures (e.g., R–454B and R-513A), the CPILMs with 40 wt % $[C_2C_1im][BF_4]$ and $[C_2C_1im][SCN]$ exhibited higher permeability of the HFCs (R-32 and R-134a, respectively) and lower permeability of the HFO R-1234yf, whose solubility in the composites was hindered due to the presence of these ILs.

On the other hand, glassy polymers with high free volume such as the polymers of intrinsic microporosity (PIMs) have gained importance over the last two decades as membrane materials for gas separation applications [14–16]. Budd et al. [17] reported on the structure of PIM-1 polymer, which they subsequently used as membrane matrices for pervaporation [18] and gas separation [19]. PIM-1 is characterised by a contorted molecular structure, resulting from the combination of the spiro-centers in the polymeric chains, and the lack of rotational freedom (lack of single bonds) along the backbone chain [20]. Consequently, it features an inflexible structure that endows a large free volume and higher microporosity in comparison with other glassy polymers, due to the low packing of the polymeric matrix [21]. As a result, PIM-1 membranes with high permeability coefficients were achieved [22], which redefined the "Robeson upper bound" limits for CO_2/CH_4 and CO_2/N_2 [23]. In view of the extraordinary separation properties of this type of material towards CO_2, herein we hypothesize that PIM-1 membranes may also show an excellent performance for the recovery of the value-added difluoromethane (R-32) from spent refrigerant mixtures, due to its comparable permeation behavior to CO_2 observed in our previous work with Pebax 1657 membranes [10,13,24,25].

Despite their outstanding separation performance, PIM-1 membranes undergo physical aging, a reversible polymer chain rearrangement due to the relaxation of the non-equilibrium polymeric chains, which implies the loss of free volume (increase chain packing) and the decay of the permeability over time, this fact being the main constraint for their industrial application [26]. In this sense, great efforts have been expended to minimize or avoid the aging phenomenon of PIM membranes by techniques such as the incorporation of inorganic fillers to the PIM-1 matrix [21,27,28]. Moreover, the topology of the PIM-1 also influences both the separation properties and the rate of physical aging [29,30].

In this work, the permeation of several single F-gases through PIM-1 membranes is assessed for the first time. To determine the effect of the PIM-1 topology in the permeation properties, the performance of the conventional PIM-1 (**B2**, predominantly disubstituted structure) membrane was compared with membranes cast from two highly branched PIM-1 polymers, high molar mass PIM-1 **B17** and lower molar mass PIM-1 **B11**. Solubility measurements were also performed and described by the dual-sorption mode model to confirm that diffusivity is governing the F-gas separation mechanism in PIM-1 membranes. Furthermore, the effects of physical aging and long-term stability of the membranes for the recovery of high purity R-32 were assessed under real mixed-gas conditions with the commercial mixtures R-410A and R–454B.

2. Experimental

2.1. PIM-1 synthesis

The materials used in the polymer synthesis are detailed in Supporting Information, Section S1. The polymer synthesis procedures employed to obtain PIM-1 polymers, **B2**, **B17** and **B11**, are outlined in Section S2. Modifications which produced branched PIM-1 samples have been previously reported in the literature [29–32], with the underpinning theory to produce highly branched PIM-1, such as **B17** and **B11**, outlined in a more recent publication [33]. The polymers were purified and then characterised as described in Section S3. The respective molar mass distributions and amount of branching present in each PIM-1 sample are presented in Table 1. **B2** denotes a predominantly disubstituted PIM-1 polymer (only 2.4% branched), whereas high molar mass **B17** (17.0%) and low molar mass **B11** (10.9%) polymers are much more highly branched PIM-1 polymers.

2.2. Membrane preparation

60–70 μm thick membranes were prepared from the PIM-1 polymer samples as follows: A 3% w/v solution of the polymer in chloroform (~0.20 g of the polymer in 6.67 mL of $CHCl_3$, pre-filtered through glass wool) was cast into a PTFE Petri dish (diameter = 6 cm) and left for 4 days at room temperature in a positive nitrogen atmosphere cabinet to allow the film to slowly form and dry. The films, which self-detached from the PTFE surface of the dish over this period of time, were then placed overnight in a vacuum oven at 120 °C to complete the drying process. The film thicknesses were confirmed with a Mitutoyo digimatic micrometer. For comparison purposes, the membranes were not soaked in methanol [34] and tested right after preparation and after a certain period of aging, as will be shown in the results sections.

2.3. Gas permeability measurements

The F-gases R-32 and R-125 as well as the mixtures R-410A (containing R-32 and pentafluoroethane, R-125 (70/30 vol%)) and R–454B (containing R-32 and 2,3,3,3-tetrafluoropropene, R-1234yf (82.94/17.06 vol%)) were supplied by Coproven Climatización (Gas Servei licensed supplier, Spain). R-134a, R-143a and R-1234yf were supplied by Carburos Metálicos (Air Products group). The single gas permeability for some of the most common refrigerant gases (R-32, R-125, R-1234yf, R-134a and R-143a), and the commercial gas mixtures (R-410A and R–454B) were assessed in a custom-made stainless-steel permeation cell of circular shape, with an effective area of 12.6 cm^2, using the flat membranes prepared as described in previous section 2.2 [10,13,24]. The feed gas flowed tangentially over the feed membrane side, and the permeate was collected using an argon sweep gas stream. Feed gas composition, flowrate and pressure were adjusted using a system of mass flowmeters and a backpressure transducer, as depicted in Fig. S8 of the Supplementary Information. The experiments were performed at a pressure of 1.3 bar on the feed side and the permeation cell was placed inside a laboratory oven at constant temperature of 30 °C. The permeate stream was analysed with a micro-gas chromatograph (Agilent 490 microGC) fitted with a PoraPLOT U column. The gas permeability coefficient was calculated according to Equation (1).

$$P_i = \frac{Q_i \cdot \delta}{A \cdot \left(f_{R,i} - f_{P,i}\right)} \tag{1}$$

where P_i (*barrer*, *1 barrer* $= 7.5 \cdot 10^{-9} \frac{cm^3_{STP}\ cm}{cm^2\ s\ bar}$) is the permeability coefficient, Q_i $(cm^3_{STP}\ s^{-1})$ is the transmembrane flow rate of gas *i* through the membrane, δ (cm) is the membrane thickness, A (cm^2) is the membrane permeation area, and $f_{R,i}$ (bar) and $f_{P,i}$ (bar) are the fugacity of component i in the retentate and permeate, respectively. The fugacity was calculated using Equation (2).

$$f_i = \varnothing_i \cdot p_i \tag{2}$$

where $\varnothing_i$ is the fugacity coefficient, calculated with REFPROP (NIST Reference Fluid Thermodynamic and Transport Properties Database) property method of Aspen Plus V11, and p_i (bar) is the partial pressure of component *i*.

Table 1
PIM-1 polymerizations used to produce polymers **B2**, **B17** and **B11**.

Polymer sample	Polymerizations (0.05 mol scale, 0.15 mol K_2CO_3)[a]					[a]*H NMR analysis*[b]	Triple detector GPC analysis[c]		
	Solvent mixture (2:1 by volume)	Polymer concentration (mol dm^{-3})	Set [average] temperature (°C)	Time (min)	Yield (%)	*Branching (%)*	M_w (kg mol^{-1})	*Đ*	Intrinsic Viscosity (cm^3 g^{-1})
B2	DMAc/DCB	0.27	160 [120]	30	97	2.4	106.2	1.8	21.8
B17	DMAc/toluene	0.27/0.21	160 [>130]	60	98	17.0	187.6	2.1	46.6
B11	DMAc/toluene	0.27/0.21	160 [130]	40	95	10.9	69.9	2.0	24.1

[a] Solvent mixture used, potential polymerization concentration at start/end, polymerization temperature, total reaction time and yield obtained in the respective polymerizations. Both B2 and B17 polymer samples exhibited low network contents (<2%), whilst B11 contained 10%.
[b] Aromatic proton integral area analysis to provide estimation of the level of branching, based on the defect peaks attributed to branch points (**c** and **d**) compared as percentage of major peaks attributed to disubstituted PIM-1 residue structures (**a** and **b**) as outlined in Table S2.
[c] Molar mass distribution analysis of polymers in chloroform to obtain weight-average molar mass (M_w), number-average molar mass (M_n) and dispersity $Đ = M_w/M_n$ for the samples.

Finally, Equation (3) presents the ideal gas selectivity ($\propto$) calculated as the ratio between the permeability coefficients of pure single gases,

$$\propto_{i/j} = \frac{P_i}{P_j} \tag{3}$$

When the feed gas was a mixture, e.g., R-410A and R–454B, the separation factor was calculated (Equation (4)) instead of the ideal gas selectivity.

$$SF = \frac{x_i^p / x_j^p}{x_i^f / x_j^f} \tag{4}$$

where x_i and x_j are the mole fractions of the compounds i and j in the binary mixture, and the superscripts p and f stand for the permeate and feed side of the membrane, respectively. Eventually, the R-32 permeate concentration in the permeate stream was calculated discounting the argon mole fraction as the ratio between R-32 mol fraction and the total mole fraction of F-gases (Equation (5)).

$$C_{R-32}(\text{vol }\%) = \frac{x_{R-32}^p}{\sum_{i=1}^{n} x_i^p} \cdot 100 \tag{5}$$

In addition, given the high permeability of the PIM-based membranes, and in order to avoid concentration polarization, the stage cut (θ), was monitored and kept below 5.5% (calculated values are reported in the Supplementary Information). The stage-cut was calculated as the ratio of permeate to feed gas flowrates, using Equation (6) for individual components (θ_i) and Equation (7) for the overall mixture permeate (θ_{Total}). The feed (20–100 $cm^3_{STP}\ min^{-1}$) and sweep gas (10–50 $cm^3_{STP}\ min^{-1}$) flowrates were independently adjusted in each experiment to minimize the value of θ, which will be shown together with the permeability data.

$$\theta_i = \frac{Q_{p,i}}{Q_f \cdot x_i^f} \tag{6}$$

$$\theta_{Total} = \frac{\sum_{i=1}^{N} Q_{p,i}}{Q_f} \tag{7}$$

2.4. Gas solubility measurements

The sorption experiments were assessed for R-32, R-125 and R-1234yf in single gas experiments at constant temperature of 30 °C, following the dual-volume pressure decay method in a custom-made sorption setup (Fig. S9) [10,24,25]. The main component of the setup is a sorption chamber (22 mL capacity stainless-steel Parr reactor), which is connected to a reservoir (50 mL capacity stainless-steel cylinder) by a valve. As the sorption experiments are performed at constant temperature, the installation is immersed in a thermostatic bath (Grant Optima TX150 heated circulating bath, temperature uniformity ±0.05 °C). Absolute pressure sensors (Keller PAA-33*X* series, 0.02% accuracy at a full scale) are used to continuously monitor and record online pressure and temperature values in the reservoir and the sorption chamber. The sorption chamber is loaded with a sample of the dense film membrane (about 0.2 g) and is subjected to desorption at high vacuum and 30 °C for 24 h, prior to each sorption test, in order to remove solvent and moisture residues. The F-gas is loaded in the reservoir at the desired pressure, while the sorption chamber is under vacuum pressure (<0.5 mbar). After the pressure and temperature have stabilized in the reservoir, the valve that connects the two compartments is opened and sorption occurs spontaneously until equilibrium is reached. The procedure is repeated, loading the reservoir at a higher pressure in each stage, until a full sorption isotherm is obtained.

Briefly, the moles of F-gas sorbed in each equilibrium step ($n_{i,j}$) were calculated as the difference between the moles initially loaded in a gas reservoir and the remaining (not absorbed) after reaching equilibrium conditions following Equation (8)

$$n_{i,j} = \rho_{(i,j,R)} \cdot V_R + \rho_{(i,j-1,S)} \cdot (V_S - V_F - V_M) - \rho_{(i,j,S)} \cdot (V_R + V_S - V_F - V_M) \tag{8}$$

where $\rho_{(i,j,R)}$, $\rho_{(i,j-1,S)}$ and $\rho_{(i,j,S)}$ are the molar densities (mol L^{-1}) of gas i in the gas reservoir, in the sorption chamber at the previous equilibrium conditions, and in the total available volume after reaching the new equilibrium conditions, respectively, and V_R, V_S, V_F and V_M are the volume (cm^3) of the gas reservoir, the sorption chamber, the dense film, and the stainless-steel mesh spacers, respectively.

The molar densities were calculated from experimental data (pressure and temperature) with the REFPROP property method available in Aspen Plus V11. Therefore, the total moles of component i sorbed in the polymer membrane for each step ($n_{i,total}$) were calculated as the moles sorbed in the last step plus the accumulated moles sorbed in the previous k steps (Equation (9)).

$$n_{i,total} = n_{i,j} + \sum_{k=1}^{j-1} n_k \tag{9}$$

The gas concentration at each equilibrium step ($C_{i,eq}$, $cm^3_{(STP)gas}\ cm^{-3}_{film}$) was calculated at standard pressure and temperature conditions (Equation (10)).

$$C_{i,eq} = \frac{22414 \cdot n_{i,total}}{V_F} \tag{10}$$

3. Results and discussion

3.1. F-gas permeability and ideal selectivity

Considering that the permeability of HFCs and HFOs in PIM-1 membranes was completely unknown beforehand, a screening of the most relevant F-gases currently used in the RAC sector, namely, R-125,

R-1234yf, R-134a, R-143a and R-32, was initially performed to elucidate their permeability behavior through three different types of PIM-1 membranes (**B2**, **B17** and **B11**) at 1.3 bar and 30 °C. In addition, the experimental system and polymer membranes used were validated by assessing the permeability of CO_2, N_2 and H_2 (Fig. S10), which were in good agreement with reported values through PIM-1 membranes cast from chloroform [34,35].

Before discussing the F-gas permeability results, we would like to draw attention to the transient behavior observed for the F-gases, depicted in Fig. S11, in contrast to the steady behavior exhibited by the non-condensable CO_2, H_2 and N_2. The time needed to reach the steady-state mass transfer rate through the PIM-1 membrane was between 60 min for R-32 (the smallest F-gas molecule) and 200 min for R-1234yf (the biggest F-gas molecule tested). Thus, this transient behavior can be attributed to the time required to stablish a steady permeation rate through the high free volume PIM-1 membranes, which for these large molecules is expected to be much higher than for common non-condensable gases owing to the expected lower diffusivity, a fact that should be confirmed with time lag measurements. For instance, Monteleone et al. (2022) [36] determined the CO_2 permeation through a PIM-DTFM-BTrip membrane and considered that a steady permeate flux was achieved from approximately 5 times the value of the time lag (around 120 s), i.e., after 10 min. Accordingly, all F-gas permeability data reported in this work correspond to experimental measurements performed after reaching stable values over time.

The F-gas permeability results through PIM-1 **B2**, PIM-1 **B17** and PIM-1 **B11**, plotted in Fig. 1a and collected in Table S3 of the Supplementary Information, reveal important differences among them. Remarkably, PIM-1 membranes show excellent R-32 permeation properties, reaching permeabilities between 1700 and 4100 barrer for the PIM-1 **B11** and PIM-1 **B2** membranes, respectively, one order of magnitude higher than through the rubbery Peba×1657 [10]. This is particularly significant because R-32 is one of the most valuable F-gases among all other third generation refrigerants, as it is one of the few HFCs that can be reused for the reformulation of new refrigeration blends of low to moderate GWP [13]. Moreover, the least permeable gas in all PIM-1 membranes is R-125 (60–145 barrer), which forms close-boiling mixtures with R-32 that are rather difficult to separate employing conventional gas separation processes. The remaining F-gases had slightly higher permeability than R-125, but much lower than R-32. As expected, these differences clearly point to a diffusion-controlled transport of the F-gases through PIM-1 membranes that favors the permeation of the one-carbon compound (R-32) over the two- and three-carbon molecules, a fact that will be confirmed with the solubility measurements discussed in Section 3.2.

Focusing on the PIM-1 membrane structures, the mostly disubstituted PIM-1 **B2** exhibited the highest permeability coefficients for most F-gases, whereas the branched polymers (PIM-1 **B17** and PIM-1 **B11**) provided significantly lower permeability coefficients, particularly for the lower molar mass PIM-1 **B11** polymer. These results show that the different PIM-1 structures have a significant impact on the permeation properties of the F-gas molecule. Both self-standing films and thin film composite gas separation membranes from more highly branched PIM-1 polymers tend to exhibit lower initial permeabilities than disubstituted samples, but then age at a much slower rate over time [29,30,32,37].

Fig. 1b presents ideal gas selectivity values calculated as the ratio of pure gas permeabilities for target F-gas systems of interest, namely, R-32/R-125 (close-boiling mixture with an azeotropic composition), R-32/R-1234yf (close-boiling mixture), and R-143a/R-125 and R-134a/R-1234yf (azeotropic mixtures). The selectivity is particularly high for the pair R-32/R-125, confirming that PIM-1 membranes may be successfully applied to the recovery of the value-added R-32, particularly for the relevant and challenging separation of R-32 from its mixtures with the HFC R-125 and the HFO R-1234yf. Unfortunately, the use of PIM-1 membranes does not seem promising for the separation of R-134a from R-1234yf. Regarding the different PIM-1 structures, the highest

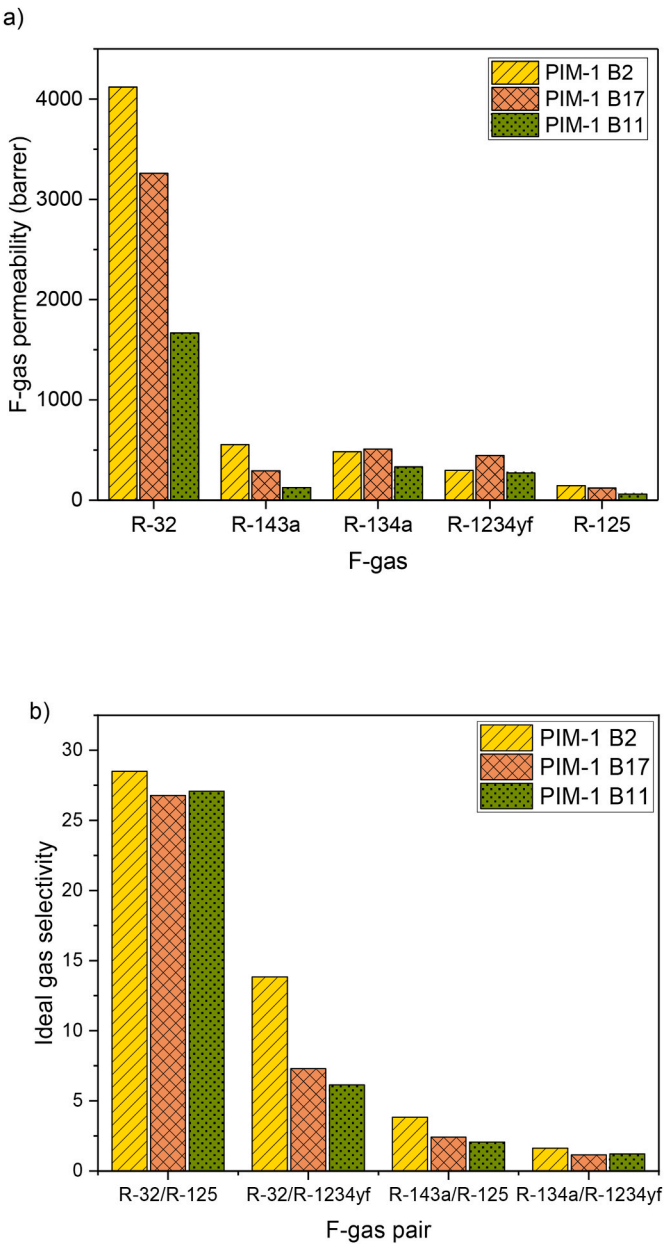

Fig. 1. a) Gas permeability of R-125, R-1234yf, R-134a, R-143a, and R-32 through PIM-1 **B2** (mostly disubstituted), PIM-1 **B17** (highly branched) and PIM-1 **B11** (branched) at 1.3 bar and 30 °C. b) Ideal gas selectivity for the gas pairs R-32/R-125, R-32/R-1234yf, R-143a/R-125, and R-134a/R-1234yf.

selectivity is obtained with the PIM-1 **B2** membrane, whereas only subtle selectivity differences are observed between PIM-1 **B17** and PIM-1 **B11** membranes. Considering these facts, together with their higher permeability, PIM-1 **B2** and PIM-1**B17** membranes were selected to assess the solubility of R-32, R-125 and R-1234yf, as well as their long-term performance to separate widespread refrigerant blends composed of those F-gases.

3.2. *F-gas sorption experiments*

Fig. 2 shows gas sorption isotherms of R-32, R-125 and R-1234yf in PIM-1 **B2** (mostly disubstituted) and PIM-1 **B17** (highly branched) at 30 °C. The upper pressure of the sorption experiments was limited by the vapor pressure of each gas (Table S1). As can be seen, the sorption isotherms of the three F-gases are concave to the pressure axis, which is

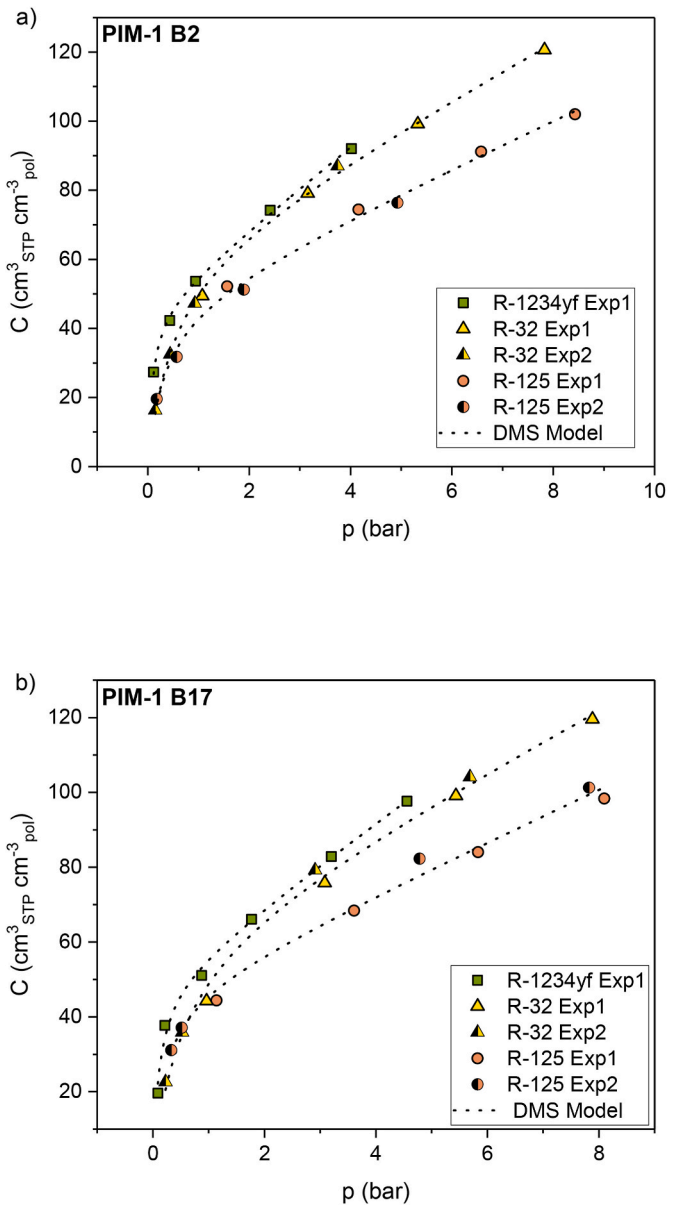

Fig. 2. Sorption isotherms of R-32, R-125 and R-1234yf in (a) PIM-1 **B2** and (b) PIM-1 **B17** at 30 °C. The dotted lines represent the dual-mode sorption (DMS) model results.

the expected behavior for glassy polymers with an initial strong sorption at low pressures (<1 bar) that corresponds to the strong sorption in the Langmuir micro-void regions. Once this region is completely filled with F-gas molecules (hole-filling process), the sorption takes place in the rest of the polymer matrix, where the solubility increases linearly following the Henry's law. Therefore, the sorption isotherms were successfully fitted ($R^2 > 0.995$) to the dual-mode sorption (DMS) model, Equation (11), which has already been applied to describe the solubility of permanent gases as well as C2 and C3 hydrocarbons in membranes prepared with PIM-1 polymers [38,39].

$$C = k_D \cdot p + \frac{C'_H \cdot b \cdot p}{1 + b \cdot p} \tag{11}$$

where C is the F-gas concentration ($cm^3_{STP}\ cm^{-3}_{pol}$), k_D the Henry's law constant ($cm^3_{STP}\ cm^{-3}_{pol}\ bar^{-1}$), C'_H the Langmuir sorption capacity ($cm^3_{STP}\ cm^{-3}_{pol}$), b the Langmuir affinity parameter (bar^{-1}), and p is the equilibrium pressure (bar) [40]. The three model parameters calculated are gathered in Table S4 of the Supplementary Information. In addition, we have fitted the experimental solubility data to the Guggenheim, Anderson and de Boer (GAB) model described by Equation (12).

$$C = \frac{v_m \cdot h \cdot p^* \cdot p}{(p^* - p) \cdot (h \cdot p + p^* - p)} \tag{12}$$

where C is the F-gas concentration ($cm^3_{STP}\ cm^{-3}_{pol}$), v_m is the capacity of the first sorption layer ($cm^3_{STP}\ cm^{-3}_{pol}$), h is the ratio of the adsorption strength in the first and the subsequent layers, p^* is a pressure independent constant (bar) and p the equilibrium pressure (bar). As in the DMS model, the GAB model is characterised by three parameters (v_m, h, p^*), which are shown in Table S5. As can be seen (Figs. S12–S13), both models fit the experimental data strikingly well. Thus, we can justify that the sorption of highly condensable gases can be described by both the DMS model and the GAB model [41,42].

The two PIM-1 **B2** and PIM-1 **B17** membranes presented high sorption capacity for all F-gases tested, the solubility of R-1234yf and R-32 being just slightly higher than that of R-125. In fact, as shown in Table S4, both PIM-1 membranes had very close DMS model parameters, so the influence of the branched structure (PIM-1 **B17**) was not reflected in the solubility of the F-gases. These sorption results are in very good agreement with the condensability of the penetrant gas, which can be

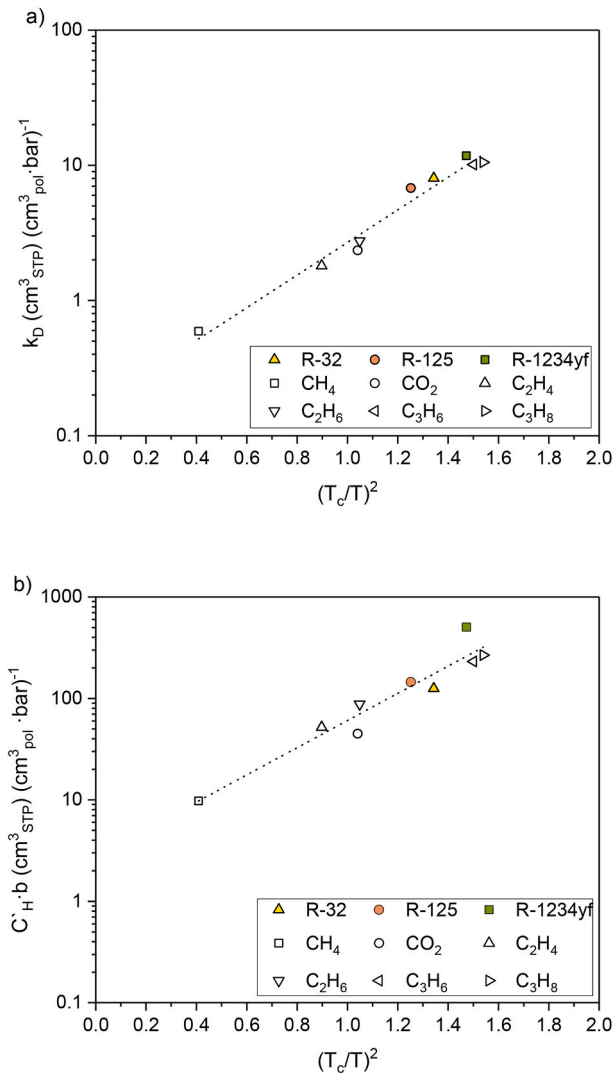

Fig. 3. Correlations of a) k_D and b) $C'_H \cdot b$ with the squared reduced critical temperature in PIM-1 **B2**. Hollow symbols are experimental data from Li et al. [34].

related to the critical temperature (T_c). In fact, as shown in Fig. 3, there is a strong correlation between the Henry and Langmuir solubility parameters (i.e., k_D and $b{\cdot}C_H$, respectively) and the squared reduced critical temperature [40,43] of the F-gases obtained in this work, which fit reasonably well to those of CO_2 and several hydrocarbons reported by Li et al. [34].

From the sorption isotherms, the F-gas solubility coefficients ($\overline{S} = C/p$) at 1.3 bar were calculated (Table 2) to determine the solubility selectivity (α_S) and diffusivity selectivity (α_D) contributions to the permselectivity of the target separations. As shown in Table 2, the solubility selectivity for the gas pairs of interest, R-32/R-125 and R-32/R-1234yf, is close to 1, the diffusivity differences among F-gases being the main factor that drives their separation in PIM-1 membranes.

3.3. Mixed-gas separation and membrane aging process

To examine the separation ability of PIM-1 membranes under mixed-gas conditions, we assessed their permeation performance towards the commercial refrigerant blend R-410A. This is an equimass mixture of R-32 and R-125, widely employed in RAC equipment over the last three decades. Furthermore, mixed gas permeation experiments were repeated with the same membrane specimens after 90 days (in the case of PIM-1 **B2**, Fig. 4a) or 124 days (for PIM-1 **B17**, Fig. 4b) to analyze the effect of membrane aging on the permeation properties of both PIM-1 membranes. In the period of time that elapsed between the two experiments, the membranes were kept in a parafilm-sealed Petri dish.

As Fig. 4 shows, the R-32 mixed-gas permeability is much higher than that of R-125, thus allowing the separation of the R-410A mixture into its components. However, compared to the ideal permeability values obtained with single gases, lower permeabilities were obtained for both compounds. In particular, the permeability of R-32 was reduced by 74% and 67% in the PIM-1 **B2** and PIM-1 **B17** membranes, respectively; whereas the permeability of R-125 decreased 54% and 17%, respectively. This behavior is not surprising and can be ascribed to competitive sorption effects in the limited non-equilibrium phase, as already reported for the mixed-gas permeability of highly condensable gases through PIM membranes [44,45], and relevant pressure-dependence permeability, as illustrated in Fig. S14, where R-32 and R-125 permeability are significantly influenced by pressure in the range 1.3–7.5 bar R-410A feed pressure of R-410A. In terms of separation performance, the permeate stream was enriched up to 97.2 and 95.8 vol % R-32 (right *y*-axis), for PIM-1 **B2** and PIM-1 **B17** membranes, respectively, from the initial feed concentration of 69.8% vol R-32. Consequently, the separation factor for the mixture R-410A was 15 and 10 in the PIM-1 **B2** and PIM-1 **B17** membranes, respectively.

In both membranes, aging phenomena reduced the permeability of both components (R-32 and R-125), likely caused by the loss of excess free volume of the membrane. However, the relaxation of the polymer matrix affected the most the permeability of larger molecules (i.e., R-125) rather than the smaller ones (i.e., R-32), as expected [46], thus enhancing the R-32/R-125 separation factor over time. In particular, the mixed-gas permeability of R-32 slightly decreased around 10%, whereas the mixed-gas permeability of R-125 was significantly affected, with a permeability drop of 60% for the PIM-1 **B2** membrane, and a slightly less marked drop (47%) for the branched PIM-1 **B17** membrane. Additionally, the aging process could be observed in the stage cut values collected in Table S7. The reduction in permeability was coupled with a decrease in the stage cut, according to the reduction of permeate flow through the membrane. As previously noted by Ameen et al. [37], PIM-1 membranes exhibiting branched structures, such as PIM-1 **B17** in this work, disturb the densification of the polymer matrix, hence, the less pronounced permeability decay of R-125 in PIM-1 **B17** membrane.

Therefore, despite the aging process, it is worth noting that the PIM-1 **B2** membrane provided very high R-32 permeability (1068 barrer) coupled to a remarkable separation factor (up to 35) of the pair R-32/R-125, which is equivalent to enriching R-32 in the gas permeate stream up to 98.8 vol %. Similarly, PIM-1 **B17** membrane presented a permeability of 930 barrer, with a lower separation factor (up to 15), which would result in a permeate concentration of 97.3 vol % R-32.

Table 2
Permeability, solubility coefficients and permeability, solubility and diffusivity selectivity for target F-gas systems in PIM-1 membranes at 1.3 bar and 30 °C.

F-gas	PIM-1 B2			PIM-1 B17		
	P, barrer	*S*, $cm^3_{STP}\ cm^{-3}_{pol}\ bar^{-1}$		*P*, barrer	*S*, $cm^3_{STP}\ cm^{-3}_{pol}\ bar^{-1}$	
R-32	4121	42		3259	42	
R-125	145	36		122	38	
R-1234yf	298	45		446	46	
Gas pair	**PIM-1 B2**			**PIM-1 B17**		
	α_P	α_S	α_D	α_P	α_S	α_D
R-32/R-125	28	1.2	24	27	1.1	24
R-32/R-1234yf	14	0.9	15	7.3	0.9	7.7

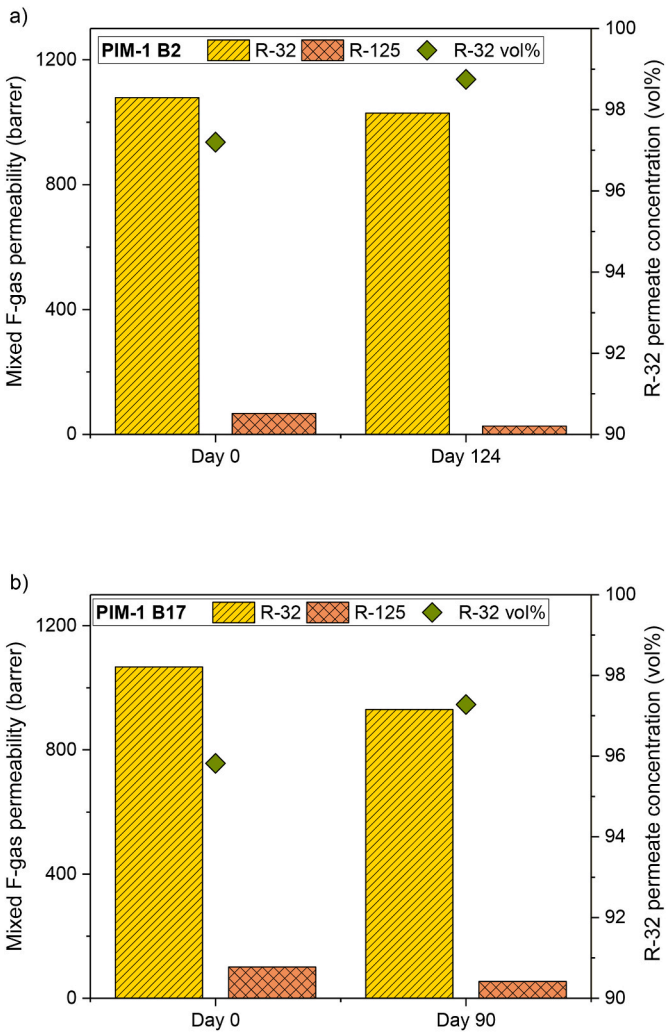

Fig. 4. Mixed-gas permeability of R-32 and R-125 (left-hand y-axis) and R-32 permeate concentration achieved (right-hand y-axis) (Equation (5)) with the freshly prepared and aged PIM-1 membranes: a) PIM-1 **B2** and b) PIM-1 **B17**. The feed gas is R-410A (an equimass mixture of R-32 and R-125) at 1.3 bar and 30 °C. Experimental data collected in Table S6.

3.4. Long-term separation performance

Yi et al. [47] reported that the aging phenomena was less severe

when long-term experiments were performed with a continuous gas feed, particularly with highly sorbing gases, as the free volume of the membrane is constantly occupied by gas, which eventually reduces the densification of the PIM-1 matrix. So, after assessing the aging process, the branched PIM-1 **B17** membrane was subjected to continuous long-term experiments with the R-410A mixture feed, at 1.3 bar and 30 °C. After four days, the feed was changed to R–454B mixture (R-32/R-1234yf, 68.9/31.1 vol %), as shown in Fig. 5.

After an initial stabilization period, the separation factor of R-410A steadily increased due to a progressive drop of R-125 permeability over time. In this sense, PIM-1 **B17** membrane reached a R-32 permeability of 1325 barrer in PIM-1 **B17**, whereas R-125 permeability dropped to 28 barrer. The decline in the permeability of R-125 led to a higher concentration of R-32 in the permeate stream, reaching a remarkable concentration of 98.9 vol %. Consequently, the separation factor of the gas pair R-32/R-125 increased to unprecedented high values around 42. When the feed was changed to R–454B, more stable permeation rates were observed over time, being the final R-32 permeability 1276 barrer, with a R-32 permeate concentration of 98.4 vol %, equivalent to a separation factor of the gas pair R-32/R-1234yf of 12. The R-32 permeability drop (from 1325 to 1244 barrer) observed when the blend is changed from R-410A to R–454B can be attributed to the different R-32 concentrations in the feed composition. The R–454B mixture has higher R-32 concentration, which implies a higher partial pressure in the feed. As is well known in glassy polymeric membranes, at low pressure ranges, an increase in feed pressure typically leads to a permeability decrease [40]. In addition, the observed higher solubility of R-1234yf relative to that of R-125 may have a greater influence on the mixed-gas permeability of R-32.

3.5. State of the art in the separation of the commercial R-410A mixture

Due to the recent interest in the recovery of high value-added F-gases, there are still few works dealing with membrane separation of the R-410A mixture for the recovery of R-32. In an attempt to compare and highlight the achievements of the present study with previous literature results, Fig. 6 presents a summary of the permeability and selectivity performance of different membranes for the separation of the R-410A mixture, in experiments done under real mixed-gas feed operation.

As can be seen, most of the previous reported results were obtained using Pebax 1657 membranes functionalized with either ILs [13] or ionNanofluids [25]. Shiflett et al. [11] reported that the use of an amorphous fluoropolymer (5% PBVE-co-95% PDD) showed superior R-32 permeability than the membranes fabricated form neat Pebax 1657 polymer. In this work, all results previously reported are significantly outperformed. The aged PIM-1 membranes achieved excellent separation factors with R-32 permeabilities above 900 barrer in long-term runs. To date, PIM-1 membranes offer the best data on the permeation properties of the R-410A mixture, in terms of both permeability and separation factor.

4. Conclusions

In this work, the study of the permeation properties of F-gases in several PIM-1 membranes was addressed for the first time, reaching permeabilities for R-32 of up to 4100 barrer coupled with high selectivity for the F-gas pairs of interest. Moreover, it was observed that PIM-1 membranes offer excellent separation properties, in terms of permeability and separation factor, in the recovery of R-32 from refrigerant gas mixtures (R-410A and R–454B). Furthermore, aged membranes achieved separation factors up to four times higher than those obtained with fresh membranes, despite a moderate loss of permeability, the branched PIM-1 **B17** structure being less affected by the aging phenomenon. Overall, PIM-1 proved to be the best material to date for the separation and recovery of almost pure R-32 from F-gas mixtures. For this reason, it is intended to move towards the development of thin film PIM-1 membranes to evaluate whether the permeation properties are maintained despite the expected much faster rate of aging.

Data statement

Data supporting this study are available within the article and supporting material.

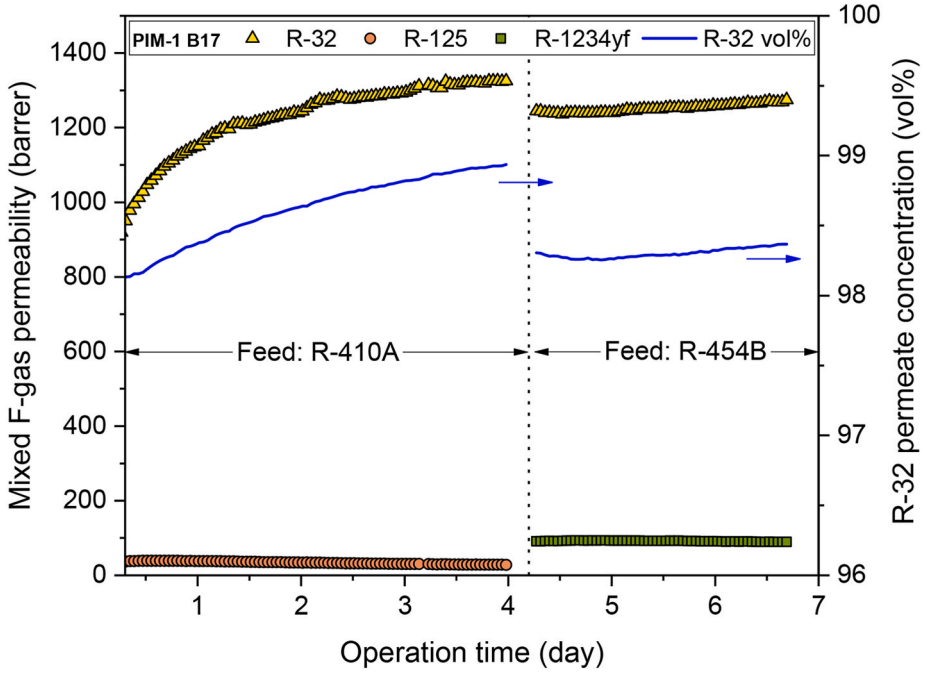

Fig. 5. Long-term mixed-gas experiment in PIM-1 **B17** membrane at 1.3 bar and 30 °C. R-410A is an equimass mixture of R-32 and R-125, and R–454B is a 69:31 wt % mixture of R-32 and R-1234yf. Symbols represent F-gas permeability data. The continuous line represents R-32 concentration in the permeate (Equation (5)).

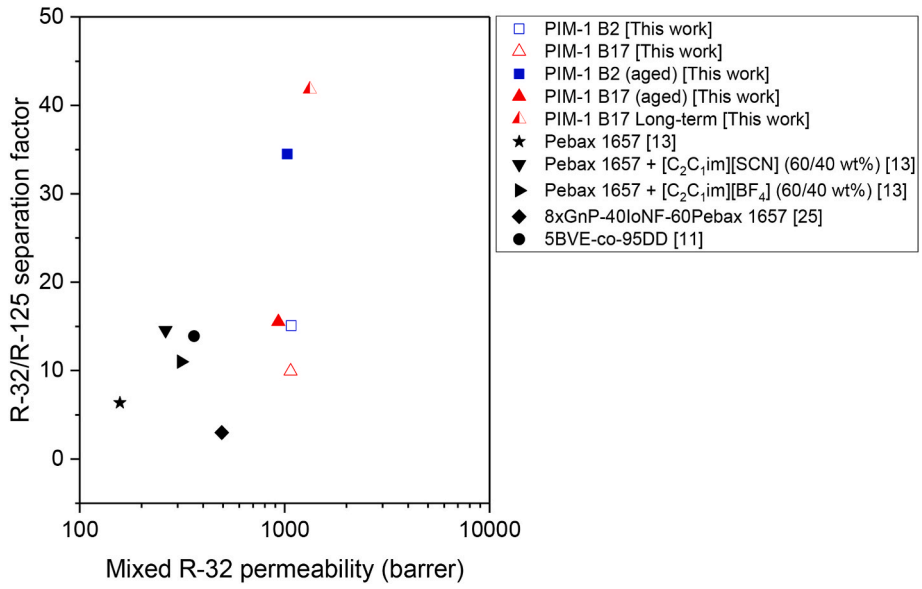

Fig. 6. Semi-logarithmic plot of R-32/R-125 selectivity vs. R-32 permeability in mixed-gas conditions. Feed gas (R-410A) is an equimass mixture of R-32 and R-125.

CRediT author statement

Sergio V. Gutiérrez-Hernández: Investigation, formal analysis, writing original draft. **Fernando Pardo**: Investigation, formal analysis, writing original draft. **Andrew Foster:** Resources, Investigation; **Peter Budd:** Resources, Investigation; **Patricia Gorgojo:** Resources, formal analysis; **Gabriel Zarca:** Conceptualization, Methodology, Writing - Review & Editing, Supervision; **Ane Urtiaga**: Conceptualization, Methodology, Funding acquisition, Writing - Review & Editing, Supervision, Project administration.

Declaration of competing interest

The authors declare that they have no known competing financial interests or personal relationships that could have appeared to influence the work reported in this paper.

Data availability

Data will be made available on request.

Acknowledgments

This research is supported by project PID2019-105827RB-I00 funded by MCIN/AEI/10.13039/501100011033. F.P. and S.V.G.H. acknowledge the support of the Spanish State Research Agency and the Spanish Ministry of Science and Innovation (grants IJC2020-043134-I and PRE2020-093568, respectively). A.B.F and P.M.B acknowledge EPSRC Grant ep/v047078/1 (SynHiSel). P.G. is supported by Grant RYC2019-027060-I funded by MCIN/AEI/10.13039/501100011033 and by "ESF Investing in your future".

Appendix A. Supplementary data

Supplementary data to this article can be found online at https://doi.org/10.1016/j.memsci.2023.121532.

References

[1] E.A. Heath, Amendment to the montreal protocol on substances that deplete the ozone layer (kigali amendment), Int. Leg. Mater. 56 (2017) 193–205, https://doi.org/10.1017/ILM.2016.2.

[2] Kyoto Protocol, Targets for the first commitment period | UNFCCC (n.d.), https://unfccc.int/process-and-meetings/the-kyoto-protocol/what-is-the-kyoto-protocol/kyoto-protocol-targets-for-the-first-commitment-period. (Accessed 21 October 2022).

[3] Regulation (EU) No 517/2014 of the European Parliament and of the Council of 16 April 2014 on fluorinated greenhouse gases and repealing Regulation (EC) No 842/2006, European environment agency (n.d.), https://www.eea.europa.eu/policy-documents/regulation-eu-no-517-2014. (Accessed 20 October 2022).

[4] S. Asensio-Delgado, F. Pardo, G. Zarca, A. Urtiaga, Absorption separation of fluorinated refrigerant gases with ionic liquids: equilibrium, mass transport, and process design, Separ. Purif. Technol. 276 (2021), 119363, https://doi.org/10.1016/j.seppur.2021.119363.

[5] A.D. Yancey, S.J. Terian, B.J. Shaw, T.M. Bish, D.R. Corbin, M.B. Shiflett, A review of fluorocarbon sorption on porous materials, Microporous Mesoporous Mater. 331 (2022), 111654, https://doi.org/10.1016/J.MICROMESO.2021.111654.

[6] D.K.J.A. Wanigarathna, J. Gao, B. Liu, Metal organic frameworks for adsorption-based separation of fluorocompounds: a review, Mater Adv 1 (2020) 310–320, https://doi.org/10.1039/d0ma00083c.

[7] J.E. Sosa, C. Malheiro, P.J. Castro, R.P.P.L. Ribeiro, M.M. Piñeiro, F. Plantier, J.P. B. Mota, J.M.M. Araújo, A.B. Pereiro, J.E. Sosa, P.J. Castro, R.P.P.L. Ribeiro, J.P. B. Mota, J.M.M. Araújo, A.B. Pereiro, C. Malheiro, F. Plantier, M.M. Piñeiro, Exploring the potential of metal–organic frameworks for the separation of blends of fluorinated gases with high global warming potential, Global Challenges (2022), 2200107, https://doi.org/10.1002/GCH2.202200107.

[8] DarshikaK.J.A. Wanigarathna, J. Gao, T. Takanami, Q. Zhang, B. Liu, Adsorption separation of R-22, R-32 and R-125 fluorocarbons using 4A molecular sieve zeolite, ChemistrySelect 1 (2016) 3718–3722, https://doi.org/10.1002/slct.201600689.

[9] J.E. Sosa, C. Malheiro, R.P. Ribeiro, P.J. Castro, M.M. Piñeiro, J.M. Araújo, F. Plantier, J.P. Mota, A.B. Pereiro, Adsorption of fluorinated greenhouse gases on activated carbons: evaluation of their potential for gas separation, J. Chem. Technol. Biotechnol. 95 (2020) 1892–1905, https://doi.org/10.1002/jctb.6371.

[10] F. Pardo, G. Zarca, A. Urtiaga, Separation of refrigerant gas mixtures containing R32, R134a, and R1234yf through poly(ether- block-amide) membranes, ACS Sustain. Chem. Eng. 8 (2020) 2548–2556, https://doi.org/10.1021/acssuschemeng.9b07195.

[11] A.N. Harders, E.R. Sturd, J.E. Vallier, D.R. Corbin, W.R. White, C.P. Junk, M. B. Shiflett, Selective separation of HFC-32 from R-410A using poly (dimethylsiloxane) and a copolymer of perfluoro(butenyl vinyl ether) and perfluoro(2,2-dimethyl-1,3-dioxole), J. Membr. Sci. 652 (2022), 120467, https://doi.org/10.1016/J.MEMSCI.2022.120467.

[12] B.D. Freeman, Basis of Permeability/Selectivity Tradeoff Relations in Polymeric Gas Separation Membranes, 1999, https://doi.org/10.1021/ma9814548.

[13] F. Pardo, G. Zarca, A. Urtiaga, Effect of feed pressure and long-term separation performance of Pebax-ionic liquid membranes for the recovery of difluoromethane (R32) from refrigerant mixture R410A, J. Membr. Sci. 618 (2021) 118744, https://doi.org/10.1016/j.memsci.2020.118744.

[14] K. Chen, L. Ni, H. Zhang, C. Xiao, L. Li, X. Guo, J. Qi, C. Wang, X. Sun, J. Li, Incorporating KAUST-7 into PIM-1 towards mixed matrix membranes with long-term stable CO2/CH4 separation performance, J. Membr. Sci. 661 (2022) 120848, https://doi.org/10.1016/J.MEMSCI.2022.120848.

[15] S. Mohsenpour, Z. Guo, F. Almansour, S.M. Holmes, P.M. Budd, P. Gorgojo, Porous silica nanosheets in PIM-1 membranes for CO2 separation, J. Membr. Sci. 661 (2022) 120889, https://doi.org/10.1016/J.MEMSCI.2022.120889.

[16] B.K. Voon, H. Shen Lau, C.Z. Liang, W.F. Yong, Functionalized two-dimensional g-C3N4 nanosheets in PIM-1 mixed matrix membranes for gas separation, Separ. Purif. Technol. 296 (2022), https://doi.org/10.1016/J.SEPPUR.2022.121354.
[17] P.M. Budd, B.S. Ghanem, S. Makhseed, N.B. McKeown, K.J. Msayib, C. E. Tattershall, Polymers of intrinsic microporosity (PIMs): robust, solution-processable, organic nanoporous materials, Chem. Commun. (2004) 230–231, https://doi.org/10.1039/B311764B, 0.
[18] P.M. Budd, E.S. Elabas, B.S. Ghanem, S. Makhseed, N.B. McKeown, K.J. Msayib, C. E. Tattershall, D. Wang, Solution-processed, organophilic membrane derived from a polymer of intrinsic microporosity, Adv. Mater. 16 (2004) 456–459, https://doi.org/10.1002/ADMA.200306053.
[19] P.M. Budd, K.J. Msayib, C.E. Tattershall, B.S. Ghanem, K.J. Reynolds, N. B. McKeown, D. Fritsch, Gas separation membranes from polymers of intrinsic microporosity, J. Membr. Sci. 251 (2005) 263–269, https://doi.org/10.1016/J.MEMSCI.2005.01.009.
[20] N.B. McKeown, P.M. Budd, Exploitation of intrinsic microporosity in polymer-based materials, Macromolecules 43 (2010) 5163–5176, https://doi.org/10.1021/MA1006396.
[21] M. Alberto, R. Bhavsar, J.M. Luque-Alled, A. Vijayaraghavan, P.M. Budd, P. Gorgojo, Impeded physical aging in PIM-1 membranes containing graphene-like fillers, J. Membr. Sci. 563 (2018) 513–520, https://doi.org/10.1016/J.MEMSCI.2018.06.026.
[22] S. He, B. Zhu, S. Li, Y. Zhang, X. Jiang, C. Hon Lau, L. Shao, Recent progress in PIM-1 based membranes for sustainable CO2 separations: polymer structure manipulation and mixed matrix membrane design, Separ. Purif. Technol. 284 (2022), 120277, https://doi.org/10.1016/J.SEPPUR.2021.120277.
[23] B. Comesaña-Gándara, J. Chen, C.G. Bezzu, M. Carta, I. Rose, M.C. Ferrari, E. Esposito, A. Fuoco, J.C. Jansen, N.B. McKeown, Redefining the Robeson upper bounds for CO 2/CH 4 and CO 2/N 2 separations using a series of ultrapermeable benzotriptycene-based polymers of intrinsic microporosity, Energy Environ. Sci. 12 (2019) 2733–2740, https://doi.org/10.1039/C9EE01384A.
[24] F. Pardo, S.v. Gutiérrez-Hernández, G. Zarca, A. Urtiaga, Toward the recycling of low-GWP hydrofluorocarbon/hydrofluoroolefin refrigerant mixtures using composite ionic liquid-polymer membranes, ACS Sustain. Chem. Eng. 9 (2021) 7012–7021, https://doi.org/10.1021/acssuschemeng.1c00668.
[25] F. Pardo, S.v. Gutiérrez-Hernández, C. Hermida-Merino, J.M.M. Araújo, M. M. Piñeiro, A.B. Pereiro, G. Zarca, A. Urtiaga, Integration of stable ionic liquid-based nanofluids into polymer membranes. Part ii: gas separation properties toward fluorinated greenhouse gases, Nanomaterials 11 (2021) 1–16, https://doi.org/10.3390/nano11030582.
[26] Z.X. Low, P.M. Budd, N.B. McKeown, D.A. Patterson, Gas permeation properties, physical aging, and its mitigation in high free volume glassy polymers, Chem. Rev. 118 (2018) 5871–5911, https://doi.org/10.1021/ACS.CHEMREV.7B00629.
[27] S. Mohsenpour, A.W. Ameen, S. Leaper, C. Skuse, F. Almansour, P.M. Budd, P. Gorgojo, PIM-1 membranes containing POSS - graphene oxide for CO2 separation, Separ. Purif. Technol. 298 (2022), 121447, https://doi.org/10.1016/J.SEPPUR.2022.121447.
[28] J.M. Luque-Alled, M. Tamaddondar, A.B. Foster, P.M. Budd, P. Gorgojo, PIM-1/Holey graphene oxide mixed matrix membranes for gas separation: unveiling the role of holes, ACS Appl. Mater. Interfaces 13 (2021), https://doi.org/10.1021/acsami.1c15640.
[29] A.B. Foster, M. Tamaddondar, J.M. Luque-Alled, W.J. Harrison, Z. Li, P. Gorgojo, P. M. Budd, Understanding the topology of the polymer of intrinsic microporosity PIM-1: cyclics, tadpoles, and network structures and their impact on membrane performance, Macromolecules 53 (2020) 569–583, https://doi.org/10.1021/ACS.MACROMOL.9B02185.
[30] A.B. Foster, J.L. Beal, M. Tamaddondar, J.M. Luque-Alled, B. Robertson, M. Mathias, P. Gorgojo, P.M. Budd, Importance of small loops within PIM-1 topology on gas separation selectivity in thin film composite membranes, J Mater Chem A Mater 9 (2021) 21807–21823, https://doi.org/10.1039/D1TA03712A.
[31] B. Qiu, M. Alberto, S. Mohsenpour, A.B. Foster, S. Ding, Z. Guo, S. Xu, S.M. Holmes, P.M. Budd, X. Fan, P. Gorgojo, Thin film nanocomposite membranes of PIM-1 and graphene oxide/ZIF-8 nanohybrids for organophilic pervaporation, Separ. Purif. Technol. 299 (2022), 121693, https://doi.org/10.1016/J.SEPPUR.2022.121693.
[32] F. Almansour, M. Alberto, A.B. Foster, S. Mohsenpour, P.M. Budd, P. Gorgojo, Thin film nanocomposite membranes of superglassy PIM-1 and amine-functionalised 2D fillers for gas separation, J Mater Chem A Mater 10 (2022) 23341–23351, https://doi.org/10.1039/D2TA06339E.
[33] S. Aloraini, M. Mathias, J. Crone, K. Bryce, M. Yu, R.A. Kirk, M.Z. Ahmad, E. D. Asuquo, S. Rico-Martínez, A.v. Volkov, A.B. Foster, P.M. Budd, Crosslinking of branched PIM-1 and PIM-py membranes for recovery of toluene from dimethyl sulfoxide by pervaporation, ACS Appl Polym Mater 5 (2022) 1145–1158, https://doi.org/10.1021/acsapm.2c01600.
[34] P. Li, T.S. Chung, D.R. Paul, Gas sorption and permeation in PIM-1, J. Membr. Sci. 432 (2013) 50–57, https://doi.org/10.1016/J.MEMSCI.2013.01.009.
[35] S. Thomas, I. Pinnau, N. Du, M.D. Guiver, Pure- and mixed-gas permeation properties of a microporous spirobisindane-based ladder polymer (PIM-1), J. Membr. Sci. 333 (2009) 125–131, https://doi.org/10.1016/J.MEMSCI.2009.02.003.
[36] M. Monteleone, A. Fuoco, E. Esposito, I. Rose, J. Chen, B. Comesaña-Gándara, C. G. Bezzu, M. Carta, N.B. McKeown, M.G. Shalygin, V.v. Teplyakov, J.C. Jansen, Advanced methods for analysis of mixed gas diffusion in polymeric membranes, J. Membr. Sci. 648 (2022), 120356, https://doi.org/10.1016/J.MEMSCI.2022.120356.
[37] A.W. Ameen, J. Ji, M. Tamaddondar, S. Moshenpour, A.B. Foster, X. Fan, P. M. Budd, D. Mattia, P. Gorgojo, 2D boron nitride nanosheets in PIM-1 membranes for CO2/CH4 separation, J. Membr. Sci. 636 (2021), 119527, https://doi.org/10.1016/J.MEMSCI.2021.119527.
[38] C.A. Scholes, J. Jin, G.W. Stevens, S.E. Kentish, Hydrocarbon solubility, permeability, and competitive sorption effects in polymer of intrinsic microporosity (PIM-1) membranes, J. Polym. Sci. B Polym. Phys. 54 (2016) 397–404, https://doi.org/10.1002/POLB.23900.
[39] P. Li, T.S. Chung, D.R. Paul, Temperature dependence of gas sorption and permeation in PIM-1, J. Membr. Sci. 450 (2014) 380–388, https://doi.org/10.1016/J.MEMSCI.2013.09.030.
[40] S. Matteucci, Y. Yampolskii, B.D. Freeman, I. Pinnau, Transport of gases and vapors in glassy and rubbery polymers, Materials Science of Membranes for Gas and Vapor Separation (2006) 1–47, https://doi.org/10.1002/047002903X.CH1.
[41] M. Lanč, K. Pilnáček, C.R. Mason, P.M. Budd, Y. Rogan, R. Malpass-Evans, M. Carta, B.C. Gándara, N.B. McKeown, J.C. Jansen, O. Vopička, K. Friess, Gas sorption in polymers of intrinsic microporosity: the difference between solubility coefficients determined via time-lag and direct sorption experiments, J. Membr. Sci. 570–571 (2019) 522–536, https://doi.org/10.1016/J.MEMSCI.2018.10.048.
[42] O. Vopička, M. Lanč, K. Friess, Phenomenology of vapour sorption in polymers of intrinsic microporosity PIM-1 and PIM-EA-TB: envelopment of sorption isotherms, Curr Opin Chem Eng 35 (2022), 100786, https://doi.org/10.1016/J.COCHE.2021.100786.
[43] A.J. Erb, D.R. Paul, Gas sorption and transport in polysulfone, J. Membr. Sci. 8 (1981) 11–22, https://doi.org/10.1016/S0376-7388(00)82135-3.
[44] R. Swaidan, B.S. Ghanem, E. Litwiller, I. Pinnau, Pure- and mixed-gas CO2/CH4 separation properties of PIM-1 and an amidoxime-functionalized PIM-1, J. Membr. Sci. 457 (2014) 95–102, https://doi.org/10.1016/J.MEMSCI.2014.01.055.
[45] E. Ricci, M.G. de Angelis, Modelling mixed-gas sorption in glassy polymers for CO2 removal: a sensitivity analysis of the dual mode sorption model, Membranes 9 (2019) 8–9, https://doi.org/10.3390/MEMBRANES9010008 (2019) 8.
[46] P. Bernardo, F. Bazzarelli, F. Tasselli, G. Clarizia, C.R. Mason, L. Maynard-Atem, P. M. Budd, M. Lanč, K. Pilnáček, O. Vopička, K. Friess, D. Fritsch, Y.P. Yampolskii, V. Shantarovich, J.C. Jansen, Effect of physical aging on the gas transport and sorption in PIM-1 membranes, Polymer (Guildf). 113 (2017) 283–294, https://doi.org/10.1016/J.POLYMER.2016.10.040.
[47] S. Yi, B. Ghanem, Y. Liu, I. Pinnau, W.J. Koros, Ultraselective glassy polymer membranes with unprecedented performance for energy-efficient sour gas separation, Sci. Adv. 5 (2019), https://doi.org/10.1126/sciadv.aaw5459.